Research Article

Journal of Molecular Recognition

Received: 19 August 2008, Revised: 25 November 2008, Accepted: 26 November 2008, Published online in Wiley InterScience: 12 January 2009

(www.interscience.wiley.com) DOI:10.1002/jmr.934

Modeling the interaction between the N-terminal domain of the tumor suppressor p53 and azurin

Monia Taranta[a], Anna Rita Bizzarri[a]* and Salvatore Cannistraro[a]

It is known that the half life of the tumor suppressor p53 can be increased by the interaction with the bacterial protein azurin, resulting in an enhanced anti-tumoral activity. The understanding of the molecular mechanisms on the basis of this phenomenon can open the way to new anti-cancer strategies. Some experimental works have given evidence of an interaction between p53 and azurin (AZ); however the binding regions of the proteins are still unknown. Recently, fluorescence studies have shown that p53 partakes in the binding with the bacterial protein by its N-terminal (NT) domain. Here we have used a computational method to get insight into this interacting mode. The model that we propose for the best complex between AZ and p53 has been obtained from a rigid-body docking, coupled with a molecular dynamics (MD) simulation, a free energy calculation, and validated by mutagenesis analysis. We have found a high degree of geometric fit between the two proteins that are kept together by several hydrophobic interactions and numerous hydrogen bonds. Interestingly, it has emerged that AZ binds essentially to the helices H_I and H_{III} of the p53 NT domain, which are also interacting regions for the foremost inhibitor of p53, MDM2. Copyright © 2009 John Wiley & Sons, Ltd.

Keywords: cancer; docking; molecular dynamics simulation; free energy

INTRODUCTION

The p53 protein plays a crucial role in maintaining the genome stability and preventing cancer development (Vogelstein *et al*., 2000). Its activation induces the expression of the genes responsible for cell cycle arrest or apoptosis, thus repairing or eliminating potentially cancerous cells (Levine, 1997). When such a cancer defence mechanism tilts, the risk of developing malignancies gets highly enhanced. The regulation of p53 is mostly accomplished by modulating its stability. Indeed, if it is true that over half of all human cancers carry mutations in the p53 gene, it is also true that tumor cells that retain wild-type p53 often display mutations in genes of factors responsible for its stabilization (Ashcroft and Vousden, 1999). Therefore, the identification of molecules that are able to restore the normal function of mutated p53, or to stabilize the wild-type, may be helpful for developing new targeted anti-cancer strategies.

Recent works have demonstrated that the copper-containing protein azurin (AZ) from the bacterium *Pseudomonas aeruginosa* can enter some human cancer cells and interact with p53, stabilizing it and inducing apoptosis through its pathway (Yamada *et al*., 2004). AZ is a small globular β-barrel protein, acting as an electron-transfer shuttle in the respiratory chain of the bacterium. It has been extensively investigated in our group by both experimental and computational approaches, to get insight into its structure, functionality, dynamics, and interaction with its natural redox partner cytochrome c551 (Bonanni *et al*., 2005; Bizzarri *et al*., 2007, 2008). AZ's potentiality of driving cancerous cells to death has been proven by Yamada *et al*. (2002), who observed that nude mice xenotransplanted with human melanoma, when treated with AZ, displayed a significant reduction in their tumor volume. Moreover, no symptoms or histologic signs of toxicity were noted in connection with AZ treatment. These results make the bacterial protein an intriguing candidate for a novel anti-tumoral therapy. However, this opportunity requires a detailed characterization of the complex between p53 and AZ, at the molecular level, to ascertain the protein interacting regions.

In our laboratory, we have explored the interaction between p53 and AZ at the level of single molecule by means of atomic force spectroscopy. The outcomes of these studies have revealed specific recognition events between p53 and AZ, with binding force and dissociation kinetics indicative of a stable complex (Taranta *et al*., 2008). However, the features of their binding and the residues involved are still little understood.

The few, known details about the structure of this complex concern some AZ residues involving its interaction with p53 (Yamada *et al*., 2002). Site-directed mutagenesis experiments indicated the residues Met^{44} and Met^{64}, located in a hydrophobic patch (HP) of AZ, as being critical for binding to the tumor suppressor.

p53 is a quite involved protein made up of four functional regions with which AZ can potentially interact: the N-terminal (NT) transactivation domain, the sequence-specific DNA binding domain (DBD), the tetramerization domain (TD), and the

* *Correspondence to: A. R. Bizzarri, Biophysics and Nanoscience Centre, CNISM, Facoltà di Scienze, Università della Tuscia, Largo dell'Università 01100, Viterbo, Italy.*
E-mail: bizzarri@unitus.it

a *M. Taranta, A. R. Bizzarri, S. Cannistraro*
Biophysics and Nanoscience Centre, CNISM, Facoltà di Scienze, Università della Tuscia, Largo dell'Università 01100, Viterbo, Italy

C-terminal (CT) regulatory domain. With the exception of the DBD that is quite well folded, the remaining regions of the protein are mostly unstructured (Bell *et al*., 2002; Dawson *et al*., 2003). The crystal structure of the full-length p53 has not been determined yet and, probably, it is just the presence of these large unfolded regions that make the crystallization process difficult.

Some experiments suggest DBD of p53 as the probable candidate to interact with AZ (Punj *et al*., 2003; De Grandis *et al*., 2007). However, also the NT domain of the tumor suppressor has been identified as a probable binding site for the bacterial protein (Punj *et al*., 2003; Apiyo and Wittung-Stafshede, 2005). In fact, a decrease in the p53-NT tryptophan emission upon AZ addition has been observed, which can be explained as an AZ Cu^{2+}-induced quenching upon binding (Apiyo and Wittung-Stafshede, 2005). Moreover, an increase in the amount of p53 secondary structure has been noted (Apiyo and Wittung-Stafshede, 2005) that, analogous to what happens with other proteins (Kussie *et al*., 1996; Bochkareva *et al*., 2005), can be justified by the AZ interaction with the NT domain of p53. This region is particularly intriguing because it is known to contain a binding site for the protein MDM2, which is the main inhibitor of p53 (Chen and Luo, 2007). To investigate the molecular details of the AZ interaction with the NT domain of p53, here we have performed a computational study, using a docking algorithm, combined with experimental mutagenesis information. We have employed the Zdock algorithm that is particularly suitable to our system, since it combines pair-wise shape complementary with desolvation and electrostatics (Chen and Weng, 2002; Chen and Weng, 2003). Finally, Molecular Dynamics (MD) and free energy calculation have been applied to select and refine the best predicted complex.

MATERIALS AND METHODS

Modeling of p53 NT

The partially unfolded p53 NT is constituted of 73 residues, organized in α-helix (H_I) and two turns assuming an α-helix structure (H_{II} and H_{III}) (see Figure 1A) when it forms a complex with other proteins. Only partial structures of NT were available from PDB: entry 1YCQ (17–27 residues), 1YCR (17–29 residues), and 2B3G (33–56 residues); the coordinates of the link between H_I and H_{II} (30–32 residues) were missing in all the entries. These entries were used to obtain a model for the 17–76 p53 sequence, by using the academic version 9v1 of MODELLER (Fiser *et al*., 2000). Fifty structures were generated and refined by a steepest descent energy minimization. Successively, they were classified on the basis of the Modeler Objective Function (MOF). The quality of the secondary structures, for the 10 models having the lowest MOF values, were analyzed by PROCHECK3.5 (Morris *et al*., 1992; Laskowski *et al*., 1993). The best found model was submitted to further refining by MD simulation to allow the relaxation of the structure.

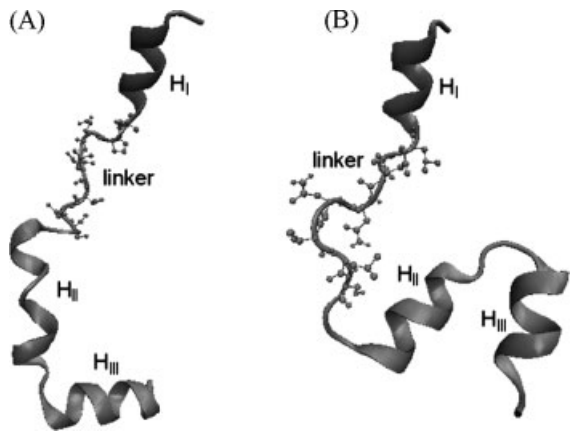

Figure 1. A: Best model for the p53 NT domain, obtained by the MODELLER software. H_I, H_{II}, and H_{III} indicate the three α-helices. Residues 30–32, missing in all the available PDB files, are shown as balls and sticks. **B**: Structure of the model as emerged after 4.5 ns of MD run.

Azurin

Initial atomic coordinates of AZ were taken from the X-ray structure at 1.93 Å resolution (chain B of PDB entry 4AZU) (Nar *et al*., 1991). The protein consists of an α-helix (H) and 8 β-strands (β_1–β_8) that form two sheets arranged in a Greek key motif (see Figure 2). The copper ion, located at the northern end of the molecule ~7 Å below the surface, is coordinated by three strong equatorial ligands (N^{δ} of His^{46} and His^{117} and S^{γ} of Cys^{112}) and two weaker axial ligands (S^{δ} of Met^{121} and the backbone oxygen of Gly^{45}). The copper ligand His^{117} is surrounded by a cluster of hydrophobic residues, known as the HP. A disulphide bridge connects residues Cys^3 and Cys^{26} in the southern region of the protein (Bonander *et al*., 2000).

Protein docking

We employed the Zdock algorithm to generate a set of possible configurations for the AZ-p53 NT complex. Zdock is a rigid-body docking algorithm using a Fast Fourier Transform (FFT) to perform an exhaustive six-dimensional search in the translational and rotational space between the two molecules (Chen and Weng, 2002; Chen and Weng, 2003). Each protein is projected into a three-dimensional grid and different values are assigned to the cells of the grid, representing the surface or the interior of the

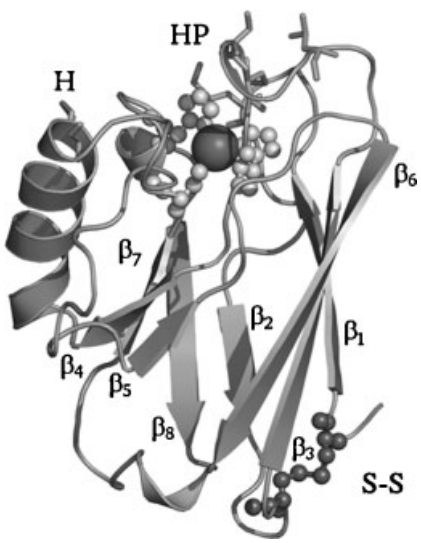

Figure 2. Three-dimensional structure of AZ. The big ball represents the copper atom, while the residues coordinating it are depicted as balls and sticks. At the opposite side the balls and sticks represent Cys^3–Cys^{26} involved in the disulphide bridge (S-S) of the protein.

Journal of Molecular Recognition

molecules. Zdock searches orientational space by rotating the ligand around its geometric center with the receptor protein kept fixed in space. For each sampled angle only the ligand translation corresponding to the best geometric match between the two proteins is retained. The obtained configurations for the complex are ranked based on a scoring function combining shape complementarity, desolvation energy, and electrostatics. The copper ion belonging to the AZ structure was included during the docking. In our simulation, AZ was kept fixed whereas the p53 NT was allowed to rotate and translate in order to explore the conformational space for the complex. Docking samplings were carried out by employing a $128 \times 128 \times 128$ point grid with a spacing of 1.2 Å and a rotational interval of 6°.

The top 2000 complexes predicted by Zdock were filtered to select binding modes consistent with the available experimental mutagenesis data. For this purpose, we applied a distance constraint between the residues at the AZ-p53 NT interface. Only those models in which both the AZ residues Met^{44} and Met^{64} are within a distance cut-off of 6 Å from the p53 NT were considered further. The filtering process reduced the number of candidate models to 135. Successively, the obtained structures were grouped in clusters to eliminate very similar conformations. For this purpose, we used the ClusPro docking server, which performs cluster analysis by means of a pairwise binding Root Mean Square Displacement (RMSD) criterion for which each group consisted of conformations differing by a maximum backbone-atoms RMSD of 6 Å from each other (Comeau *et al*., 2004). The top 20 clusters generated by ClusPro were retained for further analysis.

Molecular dynamics simulations

MD simulations were performed with the GROMACS 3.2.1 package, using the GROMOS96 43a1 forcefield (van der Spoel *et al*., 2001). Each system was solvated in a SPC water box (Berendsen *et al*., 1969) extending to atleast 6 Å from the complex surface. The MD simulations were carried out in the NPT ensemble with $T = 300$ K and $P = 1$ bar. The Nose–Hoover thermostat method was used to control the system temperature, with coupling time constant $\tau_T = 0.1$ ps. Constant pressure was imposed using the Parrinello–Rahman extended ensemble ($\tau_P = 1.0$ ps). The long-range electrostatics were treated with the Particle Mesh Ewald (PME) method with a lattice spacing of 1.2 Å. A 9 Å cut-off was employed for Lennard–Jones interactions. The pair list was updated every 10 MD steps. All covalent bonds were constrained with the LINCS algorithm (Hess *et al*., 1997). The time step was chosen to be 2 fs. The complexes were minimized with steepest descent and gradually heated from 50 to 300 K at 20 ps increments of 50 K. The systems were then equilibrated by a 600 ps MD simulation under position restraints.

For the MD run of the complex, AZ active site was modeled by applying bond harmonic potentials between the copper ion and its ligands, according to previous works (Arcangeli *et al*., 1999; Bizzarri, 2006; Bizzarri *et al*., 2007); for details see Chen and Luo (2007). The Cu ion charge was set to $q_{Cu} = 0.686$ e, giving a net AZ charge of −2.000e. By taking into account that the net charge of p53 NT is −8.000 e, 10 Na^+ ions were added to the simulation box to keep the simulated systems neutral. An unrestrained MD run was carried out for 5.5 ns. The first 1.5 ns of the run were treated as a further equilibration simulation and the remainder 4 ns were for data collection. Snapshots of the complexes were recorded every 10 ps for later binding free energy analysis.

Calculation of the binding free energy

The AZ-p53 NT interaction free energies were evaluated with the Molecular Mechanics Poisson–Boltzmann Surface Area (MM-PBSA) method (Srinivasan *et al*., 1998, De Grandis *et al*., 2007). Briefly, the procedure is based on a combination of Molecular Mechanics and continuum solvent approaches to give an estimation for the binding free energy of a protein complex: $G_{binding} = G_{complex} - G_{receptor} - G_{ligand}$, where the free energy of each term can be calculated as

$$G = E_{MM} - TS_{MM} + G_{solv} \quad (1)$$

In Equation 1 the free energy is splitted into a "gas phase" term, containing internal energy (E_{MM}) and entropic (TS_{MM}) parts, and a solvation contribution (G_{solv}), the three terms being averaged over a set of snapshots for the complex, the receptor and the ligand stored during a MD simulation. The solvation term G_{solv} can be further decomposed into electrostatic ($G_{polar,solv}$) and non-polar ($G_{non\text{-}polar,solv}$) parts (Massova and Kollman, 1999). According to what is commonly done in similar studies, we assumed that no changes occur in the receptor and ligand conformations upon binding (Ganoth *et al*., 2006; De Grandis *et al*., 2007).

The E_{MM} energy can be written as $E_{MM} = E_{elec} + E_{VdW}$, where the two terms represent the protein–protein electrostatic and Van der Waals interaction energies, respectively.

The entropic contribution to the free energy was neglected in our simulation, based on the assumption that the TS_{MM} terms for different docking modes of the same protein complex should be similar and therefore cancel out when relative binding free energies between them are calculated [32]. The electrostatic part of the solvation free energy was obtained by numerically solving the Poisson–Boltzmann equation with the Adaptive Poisson–Boltzmann Solver (APBS) software (Wu *et al*., 2004). The grid spacing was set to 0.25 Å. We used the GROMOS96 43a1 force field parameter set for atomic charges and radii and a probe radius of 1.4 Å to define the dielectric boundary. The interior dielectric constant for the complexes was 4 and the water dielectric constant was set to 80 (Ganoth *et al*., 2006). The non-polar contribution to G_{solv} was taken to be proportional to the solvent accessible surface area (SASA): $G_{non\text{-}polar,solv} = \gamma$ SASA $+ \beta$, with $\gamma = 2.2$ kJ mol^{-1}nm^{-2} and $\beta = 3.84$ kJ mol^{-1} (Chong *et al*., 1999). For each simulated complex, all calculations were averaged over 150 snapshot structures.

Computational mutagenesis

The best AZ-p53 NT binding mode was validated by investigating binding free energy changes upon replacement of the hydrophobic residues Met^{44} and Met^{64} in AZ docking interface by two polar charged residues ($Met^{44}Lys/Met^{64}Glu$), drawing on previous experimental studies about AZ-p53 complex formation (Yamada *et al*., 2002). The starting structure for the AZ-p53 NT $Met^{44}Lys/Met^{64}Glu$ complex was built from the best wild-type docking model by using the Swiss-Pdb Viewer (Guex and Peitsch, 1997). The mutant was relaxed by energy minimization followed by 3 ns MD simulation run to remove any steric conflicts. MD simulation and energetic analysis for the mutant complex were performed as described above for wt models.

Figure preparation

Figures were created with Pymol (http://pymol.sourceforge.net).

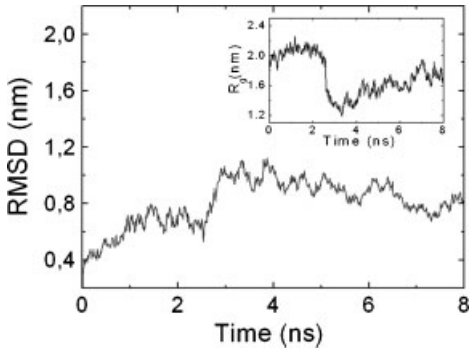

Figure 3. RMSD from the initial structure and gyration ratio (inset), as a function of time, of the p53 NT best model.

RESULTS AND DISCUSSION

Stability of the found model of p53 NT

Monitoring of the RMSD from the initial structure, as a function of time, reveals a marked upward jump around 3 ns (see Figure 3). Simultaneously, the gyration ratio exhibits a rapid drop, after which it remains almost stable (see the inset of Figure 3). At the time these events occur, the structure of p53 NT undergoes a conformational change in which the loops, linking the HI and HII helices and those between HII and HIII approach each other (see Figure 1B). This optimized structure is preserved for longer times (up to 8 ns). To perform the docking procedure, we have extracted eight snapshots from the 4.5–8 ns MD run at intervals of 0.5 ns. These snapshots were examined by PROCHECK revealing a good overall quality and conserved secondary structures.

Docking between AZ and the NT domain of p53

Starting from the structure assumed by p53 NT at 4.5 ns of the MD run (see Figure 1B), we applied the Zdock algorithm. The 2000 generated configurations for the p53 NT–AZ complex were filtered on the basis of the mutagenesis data and clustered by means of the ClusPro docking server, obtaining 20 possible complex conformations. Afterwards, the 3D structures of all these conformations were graphically compared by using the VMD software (Humphrey *et al*., 1996), resulting into five groups of complex configurations (see Figure 4). The docking procedure repeated for the other seven snapshots of the 4–5–8 ns MD run showed that, also in these cases, the generated conformations can be grouped into five clusters whose spatial arrangements are very similar to those shown in Figure 4. Such a similarity has been quantified by calculating the backbone-atom RMSD between the highest ranked models of the corresponding groups. We found that the RMSD values do not exceed 7 Å, indicating that the docking results are not very sensitive to slight changes in the p53 NT structure during the MD run after relaxation. We have therefore performed all further analysis on the snapshot at 4.5 ns.

Some of the physical properties of protein–protein interface for these five models were analyzed by the PPI server (Jones and Thornton, 1996). The results are listed in Table 1. The first column reports the interface Accessible Surface Area (ASA) values, which represent the difference in the water accessible surface area between the complex and the single proteins, providing information on the protein–protein geometric fit. A higher ASA is, in fact, an indication of a higher shape complementary between the molecules. From Table 1, we see that all the five models have ASA values included in the range of 400–1000 $Å^2$, which is characteristic of transient complexes (Nooren and Thornton, 2003). In fact, more stable complexes, such as those formed by the enzymes and their inhibitors, display a higher degree of shape complementary and ASA values between 1000 and 2000 $Å^2$ (Nooren and Thornton, 2003). We can also note that all the models are mainly characterized by non-polar interfaces between the proteins, suggesting that the stabilization of the complex is predominantly due to short-range hydrophobic interactions. Hydrogen bonds (HBs) are formed at the interface only in the case of models 4 and 7, conferring more specificity to the interaction.

If we look at the regions of the proteins involved in the interaction, we see some differences among the various models. About p53, the helices H_{II} and H_{III} are present at the binding interface in all the five docking configurations. Otherwise, the linking region that joins the helices H_I and H_{II} is involved in the interaction with AZ in all the models, with the exception of number 7. Moreover, we find the helix H_I only at the binding interface of models 2 and 7. In models 1–4, the binding also involves the linker between the helices H_{II} and H_{III}. About AZ, in all the five models the α-helix is present at the binding interface, even if the number and kind of residues involved in the interaction are not always the same. The β_4–β_5 loop is involved in binding p53 in models 1, 2, and 3, barely in model 7, while is completely excluded from the interface of model 4. Moreover we note that the β_7–β_8 loop is always present at the interface, with the exception of model 1. In model 4, and in a portion of model 3,

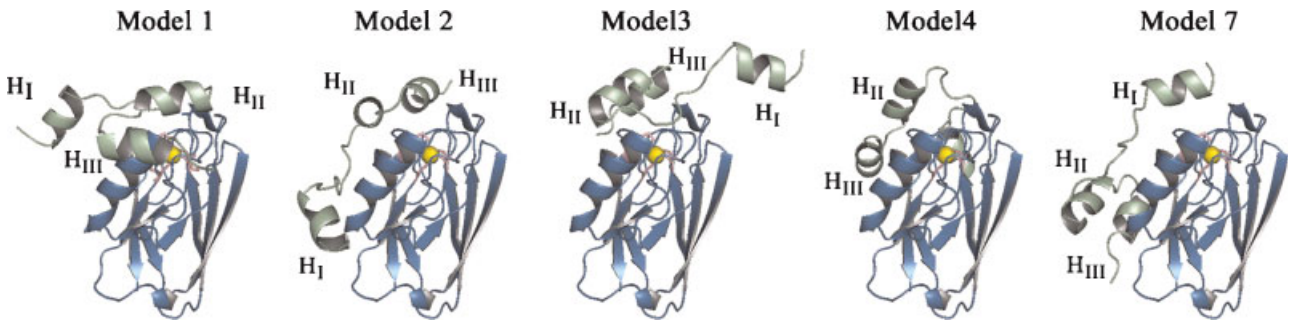

Figure 4. Three-dimensional structures of the five AZ-p53 NT complex models selected from the docking study.

Table 1. Interface parameters for the five docking models of the AZ-p53 NT complex

			p53 NT		AZ	
Model	ASA (Å^2)	HB	Polar atoms (%)	Non-polar atoms (%)	Polar atoms (%)	Non-polar atoms (%)
1	639	0	33.3	66.7	32.3	67.6
2	961	0	33.2	66.7	34.6	65.3
3	788	0	33.4	66.6	30.5	69.4
4	761	4	40.4	59.5	36.8	63.2
7	957	2	32.7	67.2	31.6	68.4

the binding surface also involves the β_1–β_2 loop. Exclusive characteristics of model 7 are the involvement of the β_2 and β_8 strands in the interaction with p53.

Molecular dynamics of the complex

The five models emerging from the docking were further investigated by MD simulations to the aim of identifying the most probable configuration of the complex, by taking into account the solvation effects and protein flexibility. In Table 2, we list the average values of the RMSD from the initial structure and the interface parameters of the models, evaluated from 100 snapshots extracted from the interval of 4.5–5.5 ns of the MD run, in which the systems were checked to be fully equilibrated. The found RMSD values, in the range of 3.5–4.7 Å, are indicative of some conformational changes occurring in the models during the MD run; these changes concerning especially the interface areas. By comparing Tables 1 and 2, we realize that the ASA value resulted essentially increased in models 1, 3, and 7, while a less pronounced increase in the ASA is observed for model 2; a decrease being instead registered for model 4. The final outcome of these changes is that now two configurations, 2 and 7, have ASA values that can be compared with those of the most stable complexes. This enhancement is probably due to the overall flexibility of the p53 NT domain that, notably in these two models, induces a conspicuous improvement in the surface matching.

The ratio of non-polar to polar residues does not undergo substantial changes during the MD run and the model interfaces remain characterized by a preponderance of non-polar interactions. In particular, the per centage of hydrophobic residues at the p53 binding interface slightly increases in models 1 and 7 and significantly in model 2. In the model 3, the p53 interface remains nearly unchanged, while in model 4 it becomes more polar. About the AZ binding surface, the amount of non-polar residues increases in model 1 and, more substantially, in model 4, while it remains almost the same in model 3 and decreases in models 2 and 7. The intermolecular interactions in aqueous environment favor the enhancement of hydrophobic residues at the interfaces, together with the molecular surface complementarity, in all the models, with the exception of model 4 in which both the ASA value and the amount of non-polar regions at the interface are reduced.

Finally, it is interesting to note that the number of HBs at the binding surface increases in all the models, with respect to the docking models, with the exception of model 4 that maintains the four HBs observed earlier. In the other models, instead, we find from five to eight new bonding interactions, which contribute to make the association between the proteins more specific.

Free energy of the interaction

More insight into the possible conformations of the complex between p53 NT and AZ has been gained by evaluating the binding free energy. The use of the MM-PBSA methodology has allowed us, moreover, to distinguish among different contributions to the whole free energy of the interaction, thus providing additional information about the character of the binding forces.

Table 2. RMSD and interface parameters for the five AZ-p53 NT models averaged over the MD simulation runs

				p53 NT		AZ	
Model	RMSD (Å)	ASA (Å^2)	HB	Polar atoms (%)	Non-polar atoms (%)	Polar atoms (%)	Non-polar atoms (%)
1	4.5 (0.1)	874 (48)	5 (2)	30.3 (3.0)	69.7 (3.0)	31.0 (4.0)	68.9 (4.0)
2	3.5 (0.1)	1016 (38)	8 (1)	26.8 (2.7)	73.1 (2.7)	35.0 (2.5)	64.9 (2.5)
3	4.7 (0.1)	898 (37)	5 (2)	33.6 (2.4)	66.3 (2.4)	30.0 (1.8)	69.9 (1.8)
4	4.3 (0.3)	584 (25)	4 (1)	41.5 (3.2)	58.4 (3.2)	31.2 (2.6)	68.8 (2.6)
7	4.5 (0.1)	1167 (30)	8 (2)	31.9 (1.7)	68.1 (1.7)	35.2 (2.3)	64.7 (2.3)

Standard deviations of averages are given in parentheses. RMSD values are calculated with respect to the complex structures at the beginning of the MD simulation (i.e., at time $t = 0$ ps).

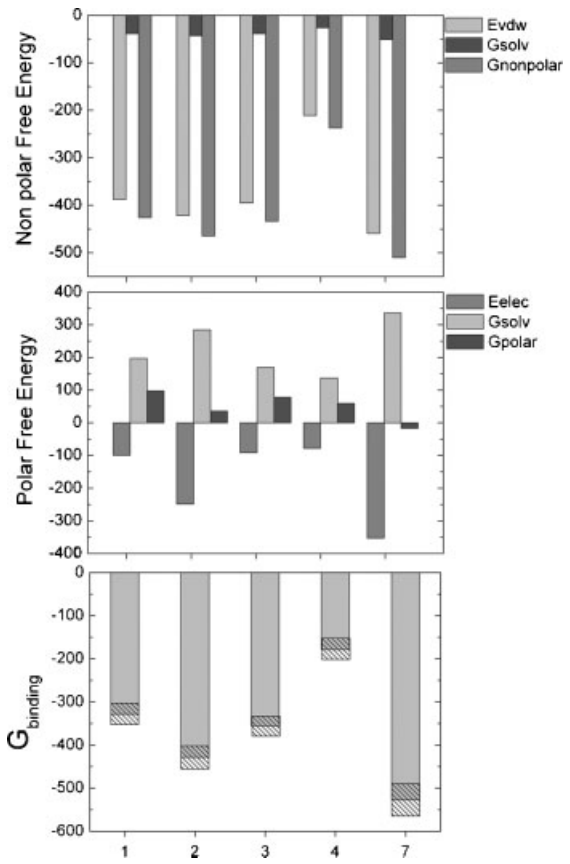

Figure 5. The three panels, from top to bottom, describe the non-polar, the polar, and the total binding free energies for the five modeled complexes. All terms were computed over 150 MD snapshots and are expressed in kJ mol^{-1}. In total binding free energies the regions pointed out by diagonal lines represent the errors.

In our study we have observed that the $G_{binding}$ of the complexes has changed in the course of time, till reaching a stable value, distinctive of each complex, as reported in the lower panel of Figure 5. This figure also displays other energy terms for the five models. In particular, in the upper panel the non-polar factors (E_{vdw}, $G_{non\text{-}polar,solv}$ and $G_{non\text{-}polar} = E_{vdw} + G_{non\text{-}polar,solv}$) and in the middle panel the polar factors (E_{elec}, $G_{polar,solv}$ and $G_{polar} = E_{elec} + G_{polar,solv}$) are represented. As we can see, in all the models the foremost contribution to the total $G_{binding}$ is due to the non-polar component, and in particular to the E_{vdw} term. The $G_{non\text{-}polar,solv}$ also contributes to favor the complex formation, even if less significantly. The highest non-polar free energy values are found for complexes 2 and 7, which are due, as observed earlier, to their high degree of surface complementarity, associated to the strong hydrophobic character of their interfaces.

The two polar components of $G_{binding}$ have a different behavior: the E_{elec} favors the complex formation whereas the $G_{polar,solv}$ favors the complex dissociation. The negative contribution to the complex formation of $G_{polar,solv}$ is the result of the desolvation of numerous buried hydrogen-bonding groups. This effect, in fact, is particularly marked for those models, as 2 and 7, which present the highest HB values during the simulations (see Table 2). The opposite contribution of the two polar terms results in a polar free energy that, in the cases of models 1, 2, 3, and 4, is unfavorable to the binding process, whereas for model 7 it contributes to promote the complex. In fact, although this model has numerous HBs, the high content in polar charged residues causes an overall G_{polar} that promotes the complex formation. In the configuration 2, the high E_{elec} value, probably due to the wide polar binding area, is nearly compensated by the highly unfavorable $G_{polar,solv}$. As a consequence, in this model the net result is a small positive G_{polar} value that unfavors the binding of the two proteins. The most disadvantageous polar free energy is instead observed for the configurations 1 and 3, where the magnitude of the desolvation term is about twice the electrostatic energy. However, the contribution of the polar free energy to $G_{binding}$ is very small for all the structures, since it represents less than 20% of the global free energy.

We can note that the ranking order of the models, based on their free energy values, changed in comparison with that obtained from the docking, thus confirming the importance of both protein flexibility and solvation effects for the specificity of protein recognition. The most probable complex conformation is now represented by model 7 that is characterized by a free energy of -527.4 kJ mol^{-1}, which is 98.7 kJ mol^{-1} more negative than the free energy associated with model 2 that is the second best prediction.

Figure 6A shows the superimposition between the three-dimensional structure of model 7 before (AZ in blue and p53 NT in aquamarine) and after (AZ in yellow and p53 NT in red) the MD simulation. As it can be noted, during the MD run the model undergoes some molecular rearrangements, which bring the p53 NT closer to AZ. In particular, we can see that the largest structural changes in the complex interface involve the helices H_{II} and H_{III} of p53. The high flexibility of the p53 NT enables these regions to adapt to the AZ shape, leading to a tight packing between the proteins. This phenomenon is clearly visible in Figure 6B, where the proteins are shown by a Van der Waals representation. The molecular rearrangements that occur during the MD run induce the establishing of numerous and favorable Van der Waals contacts, as highlighted by the magenta bar of model 7 in the upper panel of Figure 5. Many hydrophobic interactions are indeed established between the HP of AZ and p53 residues such as Phe^{19}, Leu^{22}, Trp^{23}, and Leu^{26} of the helix H_I and between Met^{56} and Met^{109} of AZ and Met^{40}, Leu^{43}, and Met^{44} of p53 H_{II} helix. Together with these interactions eight HBs are formed,

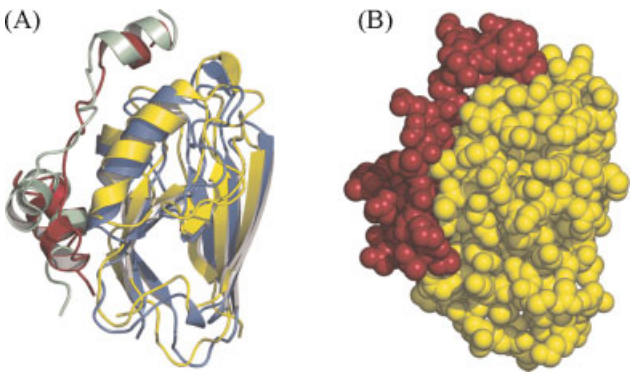

Figure 6. **A**: Superimposition of the AZ-p53 NT conformation in model 7 before (AZ in blue and p53 NT in aquamarine) and after (AZ in yellow and p53 NT in purple) the MD simulation. **B**: Van der Waals representation of model 7 as emerged after the MD run.

Table 3. Free energy of interaction for the wild-type and the mutant AZ-p53 NT complex

Model	E_{elec}	E_{vdw}	$G_{polar,solv}$	$G_{non\text{-}polar,solv}$	G_{polar}	$G_{non\text{-}polar}$	$G_{binding}$
7 wt	−353.2	−459.2	336.0	−51.0	−17.2	−510.2	−527.4
7 mutant	−328.9	−384.9	273.6	−45.2	−55.2	−430.1	−485.3

All terms are expressed in kJ mol^{-1}.

mainly involving the H_{III} helix and the short-following region of p53 and the AZ β-sheet formed by the strands β_2 and β_8. Moreover, the steric fit between the molecules is enhanced as suggested by the ASA values of model 7 reported in Tables 1 and 2.

The best predicted model has been further validated by investigating the properties of the complex binding interface after computational mutagenesis of those residues that are believed to be relevant for the protein interaction. In particular, we have taken into account the work of Yamada *et al*. which demonstrated that the substitution of the two aminoacidic residues, Met44Lys/Met64Glu yields a reduced binding affinity between the proteins (Yamada *et al*., 2002). Accordingly, we performed a computational mutagenesis by the Met44Lys/Met64Glu substitution in our best model for the complex (Model no. 7). In Table 3, the values of the various free energy components are reported. These values are in the same range as those found for other complexes involving AZ or other electron transfer proteins (Myshkin *et al*., 2005; De Grandis *et al*., 2007). The total free energy of this mutant complex turned out to be −485.3 kJ mol^{-1}, that is 42 kJ mol^{-1} less negative than the wild-type, providing a qualitative agreement with the experimental results.

The major loss in free energy is pertaining to the non-polar factor of $G_{binding}$. This is the consequence of the substitution of two non-polar residues with two charged polar ones, which leads to lose some hydrophobic interactions at the protein interface of the complex. The decrease in protein–protein Van der Waals contacts translates in a lowered degree of surface matching for the mutant model with respect to the wild-type, as can be noted by their respective ASA values.

The proposed model finds a correspondence with the experimental observation of p53 tryptophan fluorescence quenching induced by Cu^{2+} upon binding to AZ. Indeed, in our best complex configuration, Trp^{23}, which is one of the three tryptophan residues in the p53 NT, is located at the protein interface, very close to the AZ copper (∼3 Å) and thus it is expected to be quenched upon AZ binding.

If we look at the AZ-p53 NT binding mode of the selected complex, we realize that p53 partakes in the interaction by the H_I and H_{III} helices. What is noteworthy is that these helices are exactly the regions of the p53 NT domain mainly involved in the interaction with MDM2 (Kussie *et al*., 1996). This finding supports the hypothesis that AZ capability of stabilizing p53 could arise from a direct competition between the bacterial protein and the main p53 inhibitor, MDM2. In this respect, a deeper experimental investigation of the interplay between AZ and MDM2 in binding p53 could provide further relevant information.

Comparing the AZ-p53 NT complex modeled in this work with the AZ-p53 DBD best complex that resulted from our previous study (De Grandis *et al*., 2007), we note that AZ-p53 NT interaction has a free energy value (−527.4 kJ mol^{-1}) that is 124 kJ mol^{-1} more negative with respect to the AZ-p53 DBD one (−403.5 kJ mol^{-1}). This comparison suggests that the most probable configuration for the complex between AZ and p53 could involve the NT domain of the tumor suppressor. On the other hand, since more than one binding site for AZ on each p53 monomer has been proposed (Apiyo and Wittung-Stafshede, 2005), at the moment the possibility that both the configurations could take place cannot be ruled out.

CONCLUSIONS

In this work we have explored the interaction between the p53 NT domain and the bacterial protein AZ, to get insight into the molecular mechanism of a potential anti-cancer strategy. By a protein docking study, combined with MD simulations and free energy calculations, we have predicted a possible structure for a complex between these two proteins, evidencing some details about their binding sites. The model for the AZ-p53 NT complex that we propose has been further on validated by a computational mutagenesis analysis. Moreover, it is in agreement with the experimental data that reveal an AZ copper-induced fluorescence quenching of p53 tryptophans. Trp^{23} of p53, in fact, is one of the residues involved in the interaction and thus it could be reasonably quenched upon AZ binding. The protein interface is characterized by numerous hydrophobic contacts and several HBs that add specificity to the interaction, with a low free energy value and an ASA distinctive of the most stable complexes. Our results are therefore consistent with a stable binding between AZ and p53 and indicate the NT of the tumor suppressor as the domain involved in the complex formation. Remarkably, the region of p53 mainly involved in the binding contains the interacting site for MDM2. Such a finding could suggest a competition between AZ and MDM2 and inspire new approaches to engineer molecules enhancing the intracellular levels of p53.

Acknowledgements

This work has been partially supported by two PRIN-MIUR 2006 projects (no. 2006027587 and no. 2006028219). M.T. thanks the "Dipartimento di Scienza dei Materiali dell'Università di Lecce" for financial support. Thanks are due to Dr V. De Grandis for her preliminary docking investigations.

REFERENCES

Apiyo D, Wittung-Stafshede P. 2005. Unique complex between bacterial azurin and tumor-suppressor protein p53. *Biochem. Biophys. Res. Comm.* **332**: 965–968.

Arcangeli C, Bizzarri AR, Cannistraro S. 1999. Long-term molecular dynamics simulation of copper azurin: structure, dynamics and functionality. *Biophys. Chem.* **78**: 247–257.

Ashcroft M, Vousden KH. 1999. Regulation of p53 stability. *Oncogene* **18**: 7637–7643.

Baker NA, Sept D, Joseph S, Holst MJ, McCammon JA. 2001. Electrostatics of nanosystems: application to microtubules and the ribosome. *Proc. Natl. Acad. Sci. USA* **98**: 10037–10041.

Bell S, Klein C, Muller L, Hansen S, Buchner J. 2002. p53 contains large unstructured regions in its native state. *J.Mol.Biol.* **322**: 917–927.

Berendsen HJC, Postma JPM, van Gunsteren WF, Hermans J. 1969. Interaction models for water in relation to protein hydration. *Nature* **224**: 175–177.

Bizzarri AR. 2006. Topological and dynamical properties of azurin anchored to a gold substrate as investigated by molecular dynamics simulation. *Biophys. Chem.* **122**: 206–214.

Bizzarri AR, Brunori E, Bonanni B, Cannistraro S. 2007. Docking and molecular dynamics simulation of the azurin-cytochrome c551 electron transfer complex. *J. Mol. Recogn.* **20**: 122–131.

Bizzarri AR, Andolfi L, Taranta M, Cannistraro S. 2008. Optical and electronic coupling of the redox copper azurin ITO-coated quartz substrate. *Biosens. Bioelectron.* **24**: 204–209.

Bochkareva E, Kaustov L, Ayed A, Yi GS, Lu Y, Pineda-Lucena A, Liao JCC, Okorokov AL, Milner J, Arrowsmith CH, Bochkarev A. 2005. Single-stranded DNA mimicry in the p53 transactivation domain interaction with replication protein A. *Proc. Natl. Acad. Sci. USA* **102**: 15412–15417.

Bonander N, Leckner J, Guo H, Karlsson BG, Sjölin L. 2000. Crystal structure of the disulfide bond-deficient azurin mutant C3A/C26A. How important is the S-S bond for folding and stability? , *Eur. J. Biochem.* **267**: 4511–4519.

Bonanni B, Kamruzzahan ASM, Bizzarri AR, Rankl C, Gruber HJ, Hinterdorfer P, Cannistraro S. 2005. Single molecule recognition between cytochrome c551 and gold-immobilized azurin by force spectroscopy. *Biophys. J.* **89**: 2783–2791.

Chen HF, Luo R. 2007. Binding induced folding in p53-MDM2 complex. *J. Am. Chem. Soc.* **129**: 2930–2937.

Chen R, Weng Z. 2002. Docking unbound proteins using shape complementarity, desolvation, and electrostatics. *Proteins: Struct. Funct. Genet.* **47**: 281–294.

Chen R, Weng Z. 2003. A novel shape complementarity scoring function for protein–protein docking. *Proteins: Struct. Funct. Genet.* **51**: 397–408.

Chong LT, Duan Y, Wang L, Massova I, Kollman PA. 1999. Molecular dynamics and free-energy calculations applied to affinity maturation in antibody 48G7. *Proc. Natl. Acad. Sci. USA* **96**: 14330–14335.

Comeau SR, Gatchell DW, Vajda S, Camacho CJ. 2004. ClusPro: a fully automated algorithm for protein–protein docking. *Nucleic Acids Res.* **32**: 96–99.

Dawson R, Muller L, Dehner A, Klein C, Kessler H, Buchner J. 2003. The N-terminal domain of p53 is natively unfolded. *J.Mol.Biol.* **332**: 1131–1141.

De Grandis V, Bizzarri AR, Cannistraro S. 2007. Docking study and free energy simulation of the complex between p53 DNA-binding domain and azurin. *J. Mol. Recogn.* **20**: 215–226.

Fiser A, Do RK, Šali A. 2000. Modelling of loops in protein structures. *Protein Sci.* **9**: 1753–1773.

Ganoth A, Friedman R, Nachliel E, Gutman M. 2006. A molecular dynamics study and free energy analysis of complexes between the Mlc1p protein and two IQ motif peptides. *Biophys. J.* **91**: 2436–2450.

Guex N, Peitsch MC. 1997. SWISS-MODEL and the Swiss-PdbViewer: an environment for comparative protein modeling. *Electrophoresis* **18**: 2714–2723.

Hess B, Bekker H, Berendsen HJC, Fraaije JGEM. 1997. LINCS: a linear constraint solver for molecular simulations. *J. Comp. Chem.* **18**: 1463–1472.

Humphrey WF, Dalke A, Schulten K. 1996. VMD—visual molecular dynamics. *J. Mol. Graph.* **14**: 33–38.

Jones S, Thornton JM. 1996. Principles of protein–protein interactions derived from structural studies. *Proc. Natl. Acad. Sci. USA* **93**: 13–20.

Kussie PH, Gorina S, Marechal V, Elenbaas B, Moreau J, Levine AJ, Pavletich NP. 1996. Structure of the MDM2 oncoprotein bound to the p53 tumor suppressor transactivation domain. *Science* **274**: 948–953.

Laskowski RA, MacArthur MW, Moss DS, Thornton JM. 1993. PROCHECK: a program to check the stereochemical quality of protein structures. *J. Appl. Cryst.* **26**: 283–291.

Levine AJ. 1997. p53, the cellular gatekeeper for growth and division. *Cell* **88**: 323–331.

Massova I, Kollman PA. 1999. Computational alanine scanning to probe protein–protein interactions: a novel approach to evaluate binding free energies. *J. Am. Chem. Soc.* **121**: 8133–8143.

Myshkin E, Leontis NB, Bullerjahn GS. 2005. Computational simulation of the docking of prochlorothrix hollandica plastocyanin to photosystem I: modeling the electron transfer complex. *Biophys. J.* **82**: 3305–3313.

Morris AL, MacArthur MW, Hutchinson EG, Thornton JM. 1992. Stereochemical quality of protein structure coordinates. *Proteins* **12**: 345–364.

Nar H, Messerschmidt A, Huber R, van de Kamp M, Canters GW. 1991. Crystal structure analysis of oxidized Pseudomonas aeruginosa azurin at pH 5.5 and pH 9.0. A. pH-induced conformational transition involves a peptide bond flip. *J. Mol. Biol.* **221**: 765–772.

Nooren IMA, Thornton JM. 2003. Structural characterization and functional significance of transient protein-protein interactions. *J. Mol. Biol.* **325**: 991–1018.

Punj V, Das Gupta TK, Chakrabarty AM. 2003. Bacterial cupredoxin azurin and its interactions with the tumor suppressor protein p53. *Biochem. Biophys. Res. Comm.* **312**: 109–114.

Srinivasan J, Cheatham TE, Cieplak P, Kollman PA, Case DA. 1998. Continuum solvent studies of the stability of DNA, RNA, and phosphoramidate—DNA helices. *J. Am. Chem. Soc.* **120**: 9401–9409.

Taranta M, Bizzarri AR, Cannistraro S. 2008. Probing the interaction between p53 and the bacterial protein azurin by single molecule force spectroscopy. *J. Mol. Recogn.* **21**: 63–70.

van der Spoel D, van Buuren AR, Apol E, Meulenhoff PJ, Tieleman DP, Sijbers ALTM, Hess B, Feenstra KA, Lindahl E, van Drunen R, Berendsen HJC. 2001. GROMACS User Manual. University of Groningen: Groningen, The Netherlands, Version 3.2.

Vogelstein B, Lane DP, Levine AJ. 2000. Surfing the p53 network. *Nature* **408**: 307–310.

Wu Y, Cao Z, Yi H, Jiang D, Mao X, Liu H, Li W. 2004. Simulation of the interaction between ScyTx and small conductance calcium-activated potassium channel by docking and MM-PBSA. *Biophys. J.* **87**: 105–112.

Yamada T, Goto M, Punj V, Zaborina O, Chen ML, Kimbara K, Majumdar D, Cunningham E, Das Gupta TK, Chakrabarty AM. 2002. Bacterial redox protein azurin, tumor suppressor protein p53, and regression of cancer. *Proc. Natl. Acad. Sci. USA* **99**: 14098–14103.

Yamada T, Hiraoka Y, Ikehata M, Kimbara K, Avner BS, Das Gupta TK, Chakrabarty AM. 2004. Apoptosis or growth arrest: modulation of tumor suppressor p53's specificity by bacterial redox protein azurin. *Proc. Natl. Acad. Sci. USA* **101**: 4770–4775.